Parkinson's disease-associated *iPLA2-VIA*/PLA2G6 regulates neuronal functions and α-synuclein stability through membrane remodeling

Akio Mori[a], Taku Hatano[a], Tsuyoshi Inoshita[b], Kahori Shiba-Fukushima[b], Takahiro Koinuma[a], Hongrui Meng[c], Shin-ichiro Kubo[a], Spencer Spratt[a], Changxu Cui[d], Chikara Yamashita[a], Yoshimi Miki[e], Kei Yamamoto[f,g], Tetsuya Hirabayashi[h], Makoto Murakami[e,i], Yoshikazu Takahashi[i,j], Hideo Shindou[i,j,k], Takashi Nonaka[l], Masato Hasegawa[l], Ayami Okuzumi[a], Yuzuru Imai[a,d,1], and Nobutaka Hattori[a,b,c,d,1]

[a]Department of Neurology, Juntendo University Graduate School of Medicine, 113-8421 Tokyo, Japan; [b]Department of Treatment and Research in Multiple Sclerosis and Neuro-intractable Disease, Juntendo University Graduate School of Medicine, 113-8421 Tokyo, Japan; [c]Research Institute for Diseases of Old Age, Juntendo University Graduate School of Medicine, 113-8421 Tokyo, Japan; [d]Department of Research for Parkinson's Disease, Juntendo University Graduate School of Medicine, 113-8421 Tokyo, Japan; [e]Center for Disease Biology and Integrative Medicine, Graduate School of Medicine, The University of Tokyo, 113-0033 Tokyo, Japan; [f]Division of Bioscience and Bioindustry, Graduate School of Technology, Industrial and Social Sciences, Tokushima University, 770-8513 Tokushima, Japan; [g]PRIME, Japan Agency for Medical Research and Development (AMED), 100-0004 Tokyo, Japan; [h]Laboratory of Biomembrane, Tokyo Metropolitan Institute of Medical Science, 156-8506 Tokyo, Japan; [i]Japan Agency for Medical Research and Development-Core Research for Evolutionary Medical Science and Technology (AMED-CREST), AMED, 100-0004 Tokyo, Japan; [j]Department of Lipid Signaling, Research Institute, National Center for Global Health and Medicine, 162-8655 Tokyo, Japan; [k]Department of Lipid Science, Graduate School of Medicine, The University of Tokyo, 113-0033 Tokyo, Japan; and [l]Dementia Research Project, Tokyo Metropolitan Institute of Medical Science, 156-8506 Tokyo, Japan

Mutations in the *iPLA2-VIA/PLA2G6* gene are responsible for *PARK14*-linked Parkinson's disease (PD) with α-synucleinopathy. However, it is unclear how *iPLA2-VIA* mutations lead to α-synuclein (α-Syn) aggregation and dopaminergic (DA) neurodegeneration. Here, we report that *iPLA2-VIA*–deficient *Drosophila* exhibits defects in neurotransmission during early developmental stages and progressive cell loss throughout the brain, including degeneration of the DA neurons. Lipid analysis of brain tissues reveals that the acyl-chain length of phospholipids is shortened by *iPLA2-VIA* loss, which causes endoplasmic reticulum (ER) stress through membrane lipid disequilibrium. The introduction of wild-type human iPLA2-VIA or the mitochondria–ER contact site-resident protein C19orf12 in *iPLA2-VIA*–deficient flies rescues the phenotypes associated with altered lipid composition, ER stress, and DA neurodegeneration, whereas the introduction of a disease-associated missense mutant, *iPLA2-VIA* A80T, fails to suppress these phenotypes. The acceleration of α-Syn aggregation by *iPLA2-VIA* loss is suppressed by the administration of linoleic acid, correcting the brain lipid composition. Our findings suggest that membrane remodeling by iPLA2-VIA is required for the survival of DA neurons and α-Syn stability.

Parkinson's disease | lipids | *Drosophila* | ER stress | α-synuclein

Parkinson's disease (PD) is characterized by loss of the midbrain dopaminergic (DA) neurons, and its clinical features include motor symptoms and nonmotor symptoms such as akinesia, rigidity, tremor, cognitive impairment, sleep disorders, and dysautonomia (1). Pathologically, a neuronal inclusion named Lewy body (LB), which contains the presynaptic protein α-synuclein (α-Syn), ubiquitin, and lipids, is mostly observed in the affected regions, strongly implying that α-Syn aggregation is the underlying cause of neurodegeneration in PD. α-Syn presents as a natively unfolded protein and is folded as an extended α-helical structure upon binding to the acidic phospholipid surface, which suggests that the altered composition of membrane lipids could be a trigger of α-Syn aggregation (2, 3).

The nervous system is enriched in lipids and contains a more diverse lipid composition than other tissues to maintain neuronal functions (4). Within a given lipid class, different lipid species are produced from a variety of fatty acids (FAs) with different lengths and saturation levels. Among them, phospholipids have important roles in synaptic functions, vesicular transport, and organelle maintenance (5). The phospholipase A$_2$ (PLA$_2$) family consists of many subgroups of enzymes that hydrolyze the *sn*-2 ester

bonds of phospholipids, generating free fatty acids (FFAs) and lysophospholipids (6). One of the PLA$_2$ members, *PLA2G6* or *iPLA2-VIA/iPLA2β*, has been isolated as the gene responsible for an autosomal recessive form of PD linked to the *PARK14* locus (7). Postmortem examinations have revealed a marked LB pathology in *PARK14* cases (7, 8). Depending on the mutation, *iPLA2-VIA* is also the causative gene of infantile neuroaxonal dystrophy (INAD) and neurodegeneration with brain iron accumulation (NBIA) (9, 10). Thus, these 3 different neurodegenerative disorders caused by iPLA2-VIA mutations are collectively called *PLA2G6*-associated neurodegeneration (PLAN). However, the physiological substrates of iPLA2-VIA are still unclear, and it remains controversial

Significance

The mechanisms of α-synuclein aggregation and subsequent Lewy body formation are a key pathogenesis of Parkinson's disease (PD). *PARK14*-linked PD, which is caused by mutations of the *iPLA2-VIA/PLA2G6* gene, exhibits a marked Lewy body pathology. *iPLA2-VIA*, which belongs to the phospholipase A$_2$ family, is another causative gene of neurodegeneration with brain iron accumulation (NBIA). Here, we demonstrate that iPLA2-VIA loss results in acyl-chain shortening in phospholipids, which affects ER homeostasis and neurotransmission and promotes α-synuclein aggregation. The administration of linoleic acid or the overexpression of C19orf12, one of the NBIA-causative genes, also suppresses the acyl-chain shortening by *iPLA2-VIA* loss. The rescue of *iPLA2-VIA* phenotypes by C19orf12 provides significant molecular insight into the underlying common pathogenesis of PD and NBIA.

whether *PARK14*-associated iPLA2-VIA mutations affect PLA$_2$ activity (11, 12).

Phospholipids are synthesized by 2 pathways: the de novo pathway (or Kennedy pathway), using acyl-CoAs as donors; and the remodeling pathway (or Lands' cycle), in which the cycle of phospholipid deacylation and reacylation modifies the FA composition to generate a mature membrane. iPLA2-VIA has been proposed to be a key enzyme of the remodeling pathway (6, 13). Other genes responsible for NBIA, which include *Pank2*, *C19orf12*, *COASY*, and *FA2H*, are also suggested to be involved in lipid metabolism (9). However, it remains largely unknown how changes in lipid metabolism contribute to PD etiology accompanied by LB formation and NBIA pathogenesis.

In this study, we show that the loss of *iPLA2-VIA* leads to the shortening of the acyl chains of phospholipids in *Drosophila*, thereby resulting in disruption of ER homeostasis, alterations in synaptic vesicle (SV) size and neurotransmission, and DA neurodegeneration. Moreover, α-Syn loses affinity for phospholipids with shorter fatty acyl chains, facilitating α-Syn aggregation in *iPLA2-VIA*–deficient flies. Importantly, neuronal expression of NBIA-associated C19orf12 as well as wild-type (WT) human *iPLA2-VIA*, but not the pathogenic *iPLA2-VIA* mutant A80T, corrects the altered lipid composition caused by *iPLA2-VIA* loss, suppressing the neurodegenerative phenotypes of *iPLA2-VIA*–deficient flies. Thus, in addition to genetic evidence that *iPLA2-VIA* and *C19orf12* underlie a common pathogenic pathway, our results suggest that iPLA2-VIA–mediated phospholipid remodeling is a critical element for α-Syn stability and DA neuron survival.

Results

Loss of *iPLA2-VIA* Causes Degeneration of DA Neurons. CG6718 is the only iPLA2-VIA ortholog (diPLA2-VIA) in the *Drosophila* genome, showing 51% amino acid similarity to the human iPLA2-VIA (hiPLA2-VIA) (14). To determine the effects of a PD-associated iPLA2-VIA mutation on DA neuron functions, we generated *diPLA2-VIA*–null flies by CRISPR/Cas9 technology (*SI Appendix*, Fig. S1 *A* and *B*) and reintroduced hiPLA2-VIA WT or A80T in the *diPLA2-VIA*–null flies (Fig. 1*A*). Loss of diPLA2-VIA caused progressive locomotor defects and sleep disturbance (Fig. 1*B* and *SI Appendix*, Fig. S1 *C–F*). *diPLA2-VIA*$^{-/-}$ flies exhibited bang sensitivity, a seizure-and-paralysis behavior evoked by mechanical shocks (Fig. 1*C*) (15). Neuronal expression of *hiPLA2-VIA*^{WT} largely suppressed the motor and paralytic phenotypes by the loss of *diPLA2-VIA*, suggesting that hiPLA2-VIA is functional in *Drosophila* and that its activity in the central nervous system is sufficient to rescue these phenotypes (Fig. 1 *B* and *C*). In contrast, one of the *PARK14* mutants, *hiPLA2-VIA*^{A80T}, failed to rescue the neuronal phenotypes of *diPLA2-VIA*$^{-/-}$ flies (Fig. 1 *B* and *C*) (7, 16).

Consistent with the locomotion phenotype and sleep disturbance, which are partly derived from DA neuron dysfunction, the number of DA neurons in the PPL1, PPM1/2, and PPM3 clusters, as well as survivability, decreased in aged *diPLA2-VIA*$^{-/-}$ flies (*SI Appendix*, Fig. S1 *G* and *H*) (17–19). The age-dependent loss of DA neurons in *diPLA2-VIA*$^{-/-}$ flies was fully suppressed by the neuronal expression of *hiPLA2-VIA*^{WT}, whereas the expression of *hiPLA2-VIA*^{A80T} was less effective (Fig. 1 *D* and *E*). Similarly, the sleep disturbance found in *diPLA2-VIA*$^{-/-}$ flies is partially corrected by the neuronal expression of *hiPLA2-VIA*^{WT} but not of *hiPLA2-VIA*^{A80T} (*SI Appendix*, Fig. S1*I*). In contrast, the neuronal expression of *hiPLA2-VIA*^{WT} and *hiPLA2-VIA*^{A80T} on the *diPLA2-VIA*$^{-/-}$ background did not fully rescue the reduced lifespan of *diPLA2-VIA*$^{-/-}$ flies, suggesting that iPLA2-VIA activity is required for both neuronal and nonneuronal tissues (*SI Appendix*, Fig. S1*H*). To estimate whether A80T has the properties of a gain-of-function mutation, both *hiPLA2-VIA*^{WT} and *hiPLA2-VIA*^{A80T} were expressed on the *diPLA2-VIA*$^{+/+}$
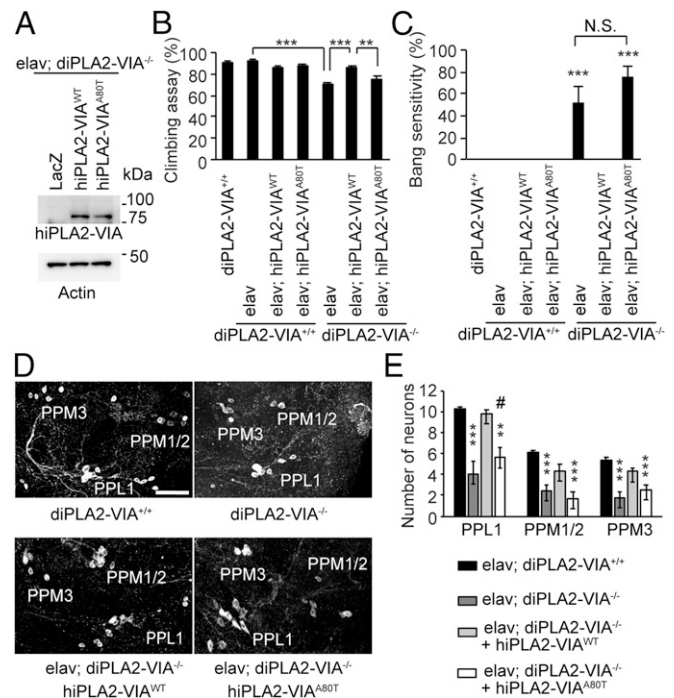

Fig. 1. Loss of iPLA2-VIA leads to DA neurodegeneration. (*A*) Complementary expression of *hiPLA2-VIA* in *diPLA2-VIA*$^{-/-}$ flies. Expression of *hiPLA2-VIA* was determined by Western blot with anti-hiPLA2-VIA. LacZ and Actin served as a mock transgene and a loading control, respectively. (*B* and *C*) Defects in motor activity and the bang-sensitive seizure phenotype of *diPLA2-VIA*$^{-/-}$ flies are fully rescued by *hiPLA2-VIA WT* but not *A80T*. The climbing assay (*n* = 20 trials in 20 male flies) and the bang test (*n* = 5 trials in 10 male flies) were performed using 5-d-old flies, and data are represented as the mean ± SEM (**$P < 0.01$ and ***$P < 0.001$ vs. any other groups in *C*) by 1-way ANOVA with the Tukey–Kramer test. N.S., not significant. (*D* and *E*) DA neurons decrease in *diPLA2-VIA*$^{-/-}$ flies, which is alleviated by *hiPLA2-VIA* expression. (*D*) The PPL1, PPM1/2, and PPM3 cluster DA neurons were visualized in 20-d-old adult brain tissues by an anti-TH antibody. (Scale bar, 50 μm.) (*E*) The number of TH-positive neurons is graphed. Data are represented as the mean ± SEM (*n* = 14 to 21 flies; **$P < 0.01$ and ***$P < 0.001$ vs. *diPLA2-VIA*$^{+/+}$; #$P < 0.05$ vs. *hiPLA2-VIA*^{WT} by 1-way ANOVA with the Tukey–Kramer test). Transgenes were driven by the pan-neuronal *elav-GAL4* driver.

background. Both flies behaved similarly to the normal control in terms of the motor and paralytic phenotypes and sleep behavior, which suggests that A80T does not have a gain-of-function property (Fig. 1 *B* and *C* and *SI Appendix*, Fig. S1*I*).

iPLA2-VIA Maintains the Phospholipid Composition in the Brain. iPLA2-VIA has been proposed to be involved in membrane homeostasis and remodeling through deacylation of phospholipids (6, 13). To determine the consequence of iPLA2-VIA loss in lipid metabolism, we analyzed the lipid composition in the brain of 20-d-old flies and found that phospholipid molecular species containing myristic acid (C14:0) or palmitoleic acid (C16:1), including phosphatidylcholine (PC) 14:0_14:0, phosphatidylethanolamine (PE) 14:0_14:0, PE 14:0_16:1, phosphatidylglycerol (PG) 14:0_16:1, and phosphatidylserine (PS) 14:0_16:1, were significantly increased, while those with acyl chains of 18:0_18:0 and 18:0_18:1, but not 18:0_18:2, were decreased (*SI Appendix*, Fig. S2 *A* and *B*). Accordingly, the ratio of acyl chain 18:0_18:X (X = 0, 1, and 2) to acyl chains 14:0_14:0 and 14:0_16:1 increased from 0.109 ± 0.003 (mean ± SEM) in the *diPLA2-VIA*$^{+/+}$ brain to 0.208 ± 0.008 in the *diPLA2-VIA*$^{-/-}$ brain (*P* = 0.0202 by Dunnett's test; Fig. 2*A*). In contrast, the amounts of lysophospholipids and FFAs such as docosahexaenoic acid (DHA), eicosapentaenoic acid, and arachidonic acid (ARA), and the proportions of PC, PE,
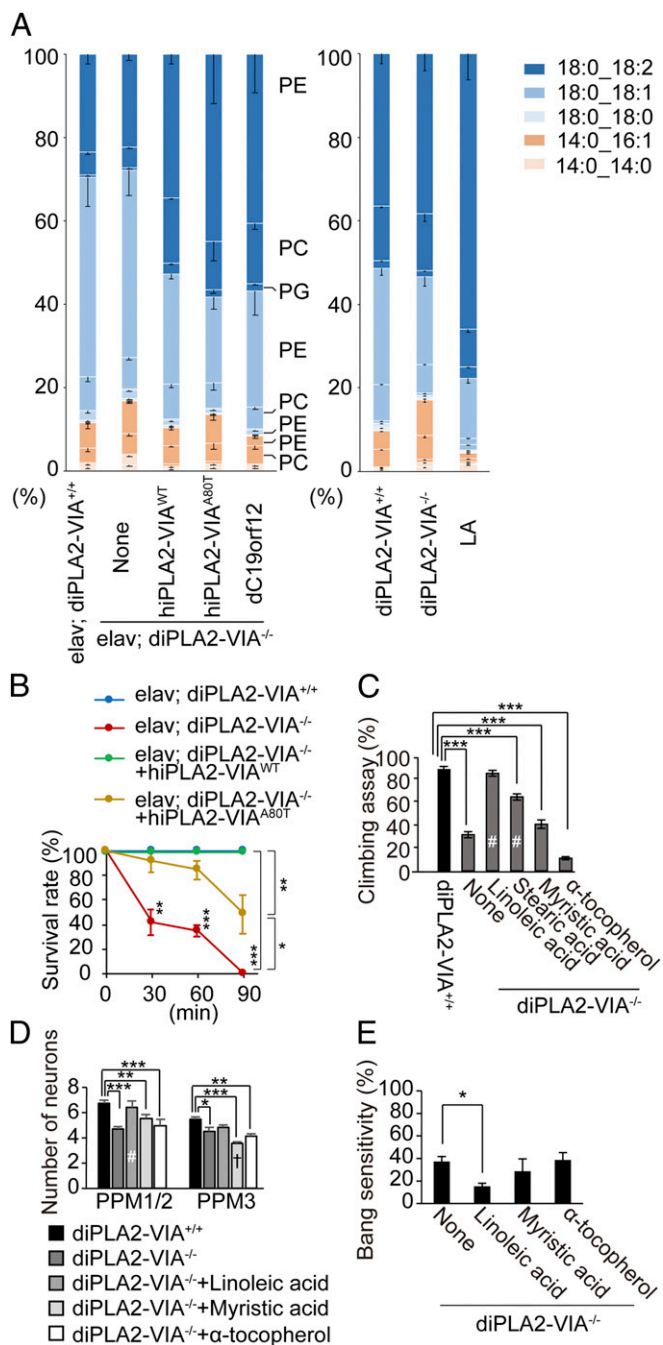
Fig. 2. *hiPLA2-VIA* introduction and linoleic acid supplementation reverse the altered lipid composition and neuronal phenotypes. (*A*) Higher rate of shorter acyl chains in *diPLA2-VIA*$^{-/-}$ and *diPLA2-VIA*$^{-/-}$ flies expressing *hiPLA2-VIA A80T*. The phospholipid composition of the *diPLA2-VIA*$^{-/-}$ brain is corrected by dC19orf12 expression or an LA-rich diet. The compositions of shorter acyl chains (14:0_14:0 and 14:0_16:1) and longer acyl chains (18:0_18:0, 18:0_18:1, and 18:0_18:2) in phospholipids and the composition of the phospholipid head groups from 20-d-old adult fly brain tissues are shown as a bar graph (mean of 3 to 4 independent samples). (*B*) *diPLA2-VIA*$^{-/-}$ flies exhibit sensitivity to high temperature. Twenty-day-old adult flies were incubated at 37 °C, and the percentage of survivors was calculated at the indicated time points (mean ± SEM, 3 trials with 10 flies; *P = 0.011, **P < 0.01, and ***P < 0.001 at each time point by 1-way ANOVA with the Tukey–Kramer test). (*C*) An LA-rich diet improves motor ability in *diPLA2-VIA*$^{-/-}$ flies. The climbing assay was performed by 3-d-old adult flies raised on normal instant fly food or an instant fly food containing FAs with different lengths of acyl chains or α-tocopherol (mean ± SEM, n = 10 to 15 flies, 20 trials; ***P < 0.001 by Dunnett's test; #P < 0.001 vs. *diPLA2-VIA*$^{-/-}$ [none]

Mori et al.

PG, and PS, were not significantly changed by *diPLA2-VIA* loss (*SI Appendix*, Fig. S2 *C* and *D*). The increased proportion of shorter acyl chains in *diPLA2-VIA*$^{-/-}$ brains was also observed at a younger age, specifically 3 d old (0.089 ± 0.013 vs. 0.057 ± 0.004 in *diPLA2-VIA*$^{+/+}$; *P* = 0.04 by 2-tailed Student's *t* test), and acyl-chain shortening appeared to be accelerated by aging (*SI Appendix*, Fig. S2E). Expression of *hiPLA2-VIA*^{WT} restored the proportion of acyl-chain composition to a normal level (0.115 ± 0.011; *P* = 0.97 vs. *diPLA2-VIA*$^{+/+}$ by Dunnett's test), whereas *hiPLA2-VIA*^{A80T} had a diminished rescue effect (0.162 ± 0.008; *P* = 0.565 vs. *diPLA2-VIA*$^{-/-}$ by Dunnett's test; Fig. 2*A*).

Membrane fluidity at a given temperature depends on the lipid class and acyl-chain composition. Decreases in the acyl-chain length lower the gel-to-liquid-crystalline phase transition temperature (20). Supporting the finding indicating a decrease in acyl-chain length, *diPLA2-VIA*$^{-/-}$ flies exhibited sensitivity to a high temperature, which was fully rescued by *hiPLA2-VIA*^{WT} but not *hiPLA2-VIA*^{A80T} (Fig. 2*B*). These data suggest that hiPLA2-VIA at least partly substituted for diPLA2-VIA in terms of lipid homeostasis and that the A80T mutant exhibited reduced function.

Dietary Manipulation of Acyl-Chain Composition Improves Neurodegeneration by *iPLA2-VIA* Loss. A dairy-containing diet influences lipid metabolism (21–23). The addition of FFAs to diet modulates the acyl-chain composition of phospholipids in fly brain tissues (24). To determine whether the alteration of phospholipids in the brain is a primary cause of neuronal phenotypes in *diPLA2-VIA*$^{-/-}$ flies, different FFAs, including linoleic acid (LA; 18:2), stearic acid (SA; 18:0), and myristic acid (MA; 14:0), were administered during a period from the hatching to adult stages. In parallel, flies were treated with α-tocopherol to prevent lipid peroxidation because elevated lipid peroxidation was observed in aged *diPLA2-VIA*$^{-/-}$ flies, as previously reported (14) (*SI Appendix*, Fig. S2F). Motor defects observed in adult *diPLA2-VIA*$^{-/-}$ flies were fully improved only by the LA-containing diet, whereas a partial improvement was observed by the SA-containing diet (Fig. 2*C*). DA neuron loss and the bang-sensitive seizure phenotype in adult *diPLA2-VIA*$^{-/-}$ flies were also rescued by a diet containing LA but not by a diet containing MA or α-tocopherol (Fig. 2 *D* and *E*). Consistent with the improvement of neuronal phenotypes, measurement of brain lipid composition revealed that the LA-containing diet decreased the proportion of phospholipids with shorter acyl chains in *diPLA2-VIA*$^{-/-}$ flies (0.047 ± 0.0007; *P* = 0.0004 vs. *diPLA2-VIA*$^{-/-}$ by Dunnett's test; Fig. 2*A*). However, LA supplementation was unable to fully rescue the reduced lifespan of diPLA2-VIA$^{-/-}$ flies, which once again suggested the nonneuronal roles of iPLA2-VIA (*SI Appendix*, Fig. S1H).

Mitochondrial degeneration has been reported in *iPLA2-VIA*–deficient *Drosophila* and mice (14, 25). We examined whether membrane lipid disequilibrium caused by iPLA2-VIA loss also affects mitochondrial activity. However, brain ATP content was not changed, and mitochondrial morphology in both DA neurons and indirect flight muscles, which is readily compromised by mutations of mitochondria-associated PD genes such as *PINK1* and *CHCHD2*, was also normal (*SI Appendix*, Fig. S2 *G–I*) (26, 27). In addition, LA supplementation failed to rescue the motor defects and DA neuron loss in *CHCHD2*- or *PINK1*-deficient flies (*SI Appendix*, Fig. S2 *J* and *K*). Together, these data suggest

by 1-way ANOVA with the Tukey–Kramer test). (*D*) An LA-rich diet rescues DA neuron loss caused by lack of *diPLA2-VIA*. The number of DA neurons in each cluster in 20-d-old adult flies (mean ± SEM, n = 11 to 23; *P < 0.05, **P < 0.01, and ***P < 0.001 by Dunnett's test; †P < 0.005 and #P < 0.001 vs. *diPLA2-VIA*$^{-/-}$ by 1-way ANOVA with the Tukey–Kramer test). (*E*) The bang-sensitive seizure-paralysis phenotype of 5-d-old *diPLA2-VIA*$^{-/-}$ flies is rescued by LA supplementation. Data are represented as the mean ± SEM (n = 10 male flies, 4 trials; *P < 0.05 by Dunnett's test).

that the alteration of brain lipid composition contributes to PLAN-linked neurodegeneration and that mitochondrial degeneration is not a primary cause of PLAN-linked neurodegeneration.

MPAN-Associated C19orf12 Rescues Neuronal Phenotypes Caused by iPLA2-VIA Loss.

Mutations in the *C19orf12* gene are associated with mitochondrial membrane protein-associated neurodegeneration (MPAN), an autosomal-recessive disorder that accounts for 5 to 30% of NBIA cases (9). Similar to PD patients, both PLAN and MPAN patients show a common LB pathology (7, 8, 28). In addition to the pathological similarity, C19orf12 has been suggested to be involved in lipid metabolism (9). One of the neuronal phenotypes of *diPLA2-VIA⁻/⁻* flies is bang sensitivity, which has also been reported in *C19orf12*-knockdown flies (29, 30). Neuronal overexpression of the *C19orf12* homolog CG3740 (*dC19orf12*) rescued the heat sensitivity, motor disability, and bang sensitivity of *iPLA2-VIA⁻/⁻* flies (Fig. 3 *A–C* and *SI Appendix,* Fig. S3*A*). *dC19orf12* overexpression also suppressed DA neuron loss of *diPLA2-VIA⁻/⁻* flies and partially improved their sleep disturbance (Fig. 3*D* and *SI Appendix,* Fig. S1*I*). Brain vacuolar formation caused by *diPLA2-VIA* loss, which has also been reported pre-viously (14), was suppressed by *dC19orf12* as well as *hiPLA2-VIA^WT* (Fig. 3 *E* and *F*). Consistent with the rescuing effects on neurodegeneration-associated phenotypes, the increased proportion of shorter acyl chains in phospholipids was corrected to a normal level by *dC19orf12* expression (0.099 ± 0.029; *P* = 0.589 vs. *diPLA2-VIA⁺/⁺* by Dunnett's test; Fig. 2*A*). These observations suggest that iPLA2-VIA and C19orf12 act, at least in part, in the same pathway for lipid metabolism.

iPLA2-VIA appears to show dynamic localization to the mitochondria and the ER and has some roles in the membranes of these organelles (14, 25, 30–32). The salivary gland of the *diPLA2-VIA⁻/⁻* mutant was poorly developed, and the ER areas of the gland were extended, suggesting that its ER functions were greatly compromised (Fig. 3*G* and *SI Appendix,* Fig. S3*B*). Altered lipid composition of the ER membrane activates the ER stress transducer IRE1, which up-regulates the ER stress-associated transcriptional activator XBP1 through processing of the *XBP1* mRNA precursor (33). Suppression of acyl-chain shortening in phospholipids by LA treatment mitigated the morphological defect of the ER and suppressed XBP1 activation by diPLA2-VIA loss, which indicates that membrane lipid
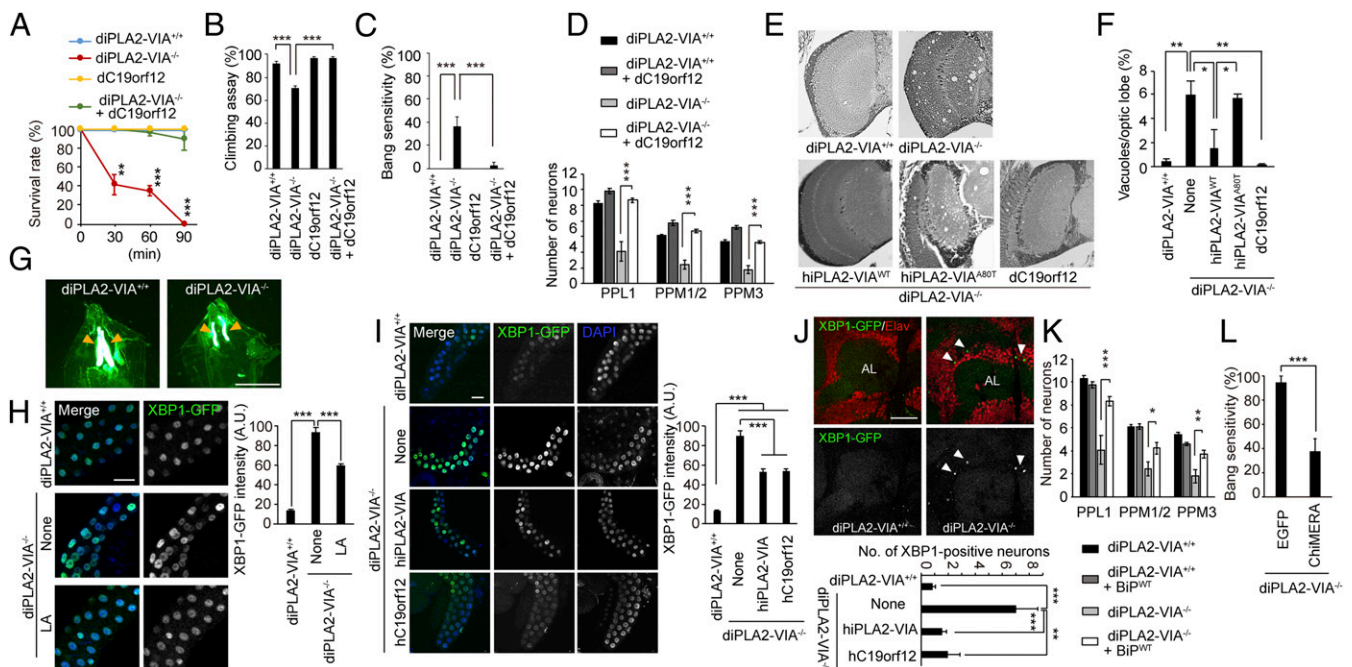

Fig. 3. Neurodegeneration of *diPLA2-VIA⁻/⁻* flies is rescued by MPAN-associated C19orf12. (*A*) Neuronal expression of the MPAN-associated gene *dC19orf12* improves sensitivity to high temperature. The assay was performed as described in Fig. 2*B* (mean ± SEM, 3 trials with 10 flies at 20 d old; **P < 0.001 and ***P < 0.0001 by 1-way ANOVA with the Tukey–Kramer test). (*B* and *C*) Neuronal expression of *dC19orf12* rescues motor disability and bang-sensitive seizures in *iPLA2-VIA⁻/⁻* flies. The climbing (mean ± SEM, *n* = 10 to 15 flies, 20 trials) and bang sensitivity (mean ± SEM, *n* = 30 to 40 flies) assays were performed with 3-d-old adult flies (***P < 0.0001 by 1-way ANOVA with the Tukey–Kramer test). (*D*) *dC19orf12* rescues DA neuron loss caused by lack of *diPLA2-VIA.* The number of DA neurons in the indicated clusters is graphed (mean ± SEM, *n* = 12 to 22 flies at 20 d old; ***P < 0.0001 by 1-way ANOVA with the Tukey–Kramer test). (*E* and *F*) Expression of *hiPLA2-VIA* WT and *dC19orf12* suppresses the vacuolation of the *diPLA2-VIA⁻/⁻* fly brain. (*E*) Light-microscopic examination of brain tissue sections from 20-d-old flies with the indicated genotypes. (*F*) The percentage of total vacuole areas accounting for the optic lobe regions is graphed (mean ± SEM, *n* = 3 flies; *P < 0.05 and **P < 0.01 by 1-way ANOVA with the Tukey–Kramer test). (*G*) Poor development of salivary glands (arrows) caused by lack of *diPLA2-VIA.* The salivary glands at the third-instar larval stage were visualized by ER-mAG1. (Scale bar, 1 mm.) (*H* and *I*) ER stress in the salivary glands of the *diPLA2-VIA⁻/⁻* larvae is improved by LA (1 μL/mL) treatment or by the expression of *hiPLA2-VIA* or *dC19orf12.* XBP1-GFP and DAPI images in the salivary glands of third-instar larvae with the indicated genotypes. (Scale bars, 50 μm.) Graphs represent XBP1-GFP signal intensities with the indicated genotypes (*n* = 142 to 526 cells in 3 to 12 larvae; ***P < 0.001 by 1-way ANOVA with the Tukey–Kramer test). (*J*) Neuronal ER stress caused by iPLA2-VIA loss is relieved by the expression of *hiPLA2-VIA* or *dC19orf12.* Images show XBP1-GFP and Elav from an anterior view in the brains of 20-d-old flies. (Scale bar, 50 μm.) Arrowheads indicate XBP1- and Elav-positive signals. Elav was used as a neuron-specific nuclear marker. AL, antennal lobe. Graph represents the number of XBP1-GFP–positive neurons per brain (*n* = 9 to 13 flies; **P < 0.005 and ***P < 0.001 by 1-way ANOVA with the Tukey–Kramer test). (*K*) DA neuron loss caused by lack of *diPLA2-VIA* is improved by WT BiP (BiP^WT) in *diPLA2-VIA⁻/⁻* flies at 20 d old. The number of DA neurons in the indicated clusters is graphed (mean ± SEM, *n* = 7 to 15 flies; *P < 0.01, **P < 0.001, and ***P < 0.0001 by 1-way ANOVA with the Tukey–Kramer test). (*L*) The bang-sensitive seizure phenotype is rescued by ChiMERA but not EGFP in *diPLA2-VIA⁻/⁻* flies at 20 d old. Data are represented as the mean ± SEM (*n* = 17 EGFP and *n* = 33 ChiMERA flies; ***P < 0.001 by 2-tailed Student's *t* test).

disequilibrium caused by iPLA2-VIA loss evokes ER stress (Fig. 3*H* and *SI Appendix*, Fig. S3*B*). The ER morphological defect and XBP1 activation were also mitigated by *hiPLA2-VIA*^{WT} or *hC19orf12* expression (Fig. 3*I* and *SI Appendix*, Fig. S3*B*). Additionally, sporadic XBP1 activation in neurons was observed in the aged *diPLA2-VIA*$^{-/-}$ fly brain and suppressed by *hiPLA2-VIA*^{WT} or *hC19orf12* expression (Fig. 3*J*). IER1 oligomerization and activation are negatively regulated by the ER chaperone BiP (34). The neuronal expression of *Drosophila* BiP (or Hsc70-3) improved DA neuron loss due to the lack of diPLA2-VIA (Fig. 3*K*). BiP overexpression also ameliorated the bang-sensitivity phenotype and motor defects through diPLA2-VIA loss (*SI Appendix*, Fig. S3 *C* and *D*). Again, these results suggest that altered lipid composition caused by iPLA2-VIA loss induces ER stress, presumably leading to widespread neurodegeneration in addition to DA neuron degeneration.

We next examined the mechanism by which C19orf12 rescues ER stress. hC19orf12 has been found at the mitochondria-associated ER membrane (MAM), among other locations, and we confirmed that hC19orf12^{WT} is localized at the MAM as well as the ER and mitochondria in cultured human cells (*SI Appendix*, Figs. S3 *E*, *F*, and *H*) (35). In contrast, the MPAN-associated hC19orf12^{G69R} mutant completely lost its localization to the ER and mitochondria (*SI Appendix*, Fig. S3*H*). hiPLA2-VIA^{WT} and hiPLA2-VIA^{A80T} were largely localized in the cytoplasm of cultured human cells, as small dot-like structures and hiPLA2-VIA^{WT} but not hiPLA2-VIA^{A80T} appeared to show partial colocalization with the ER (*SI Appendix*, Fig. S3*I*). Although we did not detect a physical interaction or colocalization between hiPLA2-VIA and hC19orf12 (*SI Appendix*, Fig. S3 *G* and *J*), overexpression of hC19orf12^{WT} increased the number of MAMs, while hC19orf12^{G69R} failed to do so (*SI Appendix*, Fig. S3*K*). To confirm whether enhanced MAM integrity by C19orf12 rescues ER defects of *diPLA2-VIA*$^{-/-}$ flies, we employed the protein ChiMERA, which consists of the mitochondrial Tom70 fused to the ER protein Ubc6 and GFP and up-regulates MAM (36). The enhancement of MAM integrity by ChiMERA also rescued the bang-sensitive seizure phenotype of *diPLA2-VIA*$^{-/-}$ flies, suggesting that enhanced MAM integrity alleviates the defects in neuronal activity by correcting membrane lipid disequilibrium (Fig. 3*L*). However, ChiMERA expression failed to rescue DA neuron loss in *diPLA2-VIA*$^{-/-}$ flies, which suggests that there exists a dynamic regulatory mechanism of C19orf12 in terms of MAM formation in response to neuronal activity or that C19orf12 has additional functions in maintaining the survival of DA neurons (*SI Appendix*, Fig. S3*L*).

Alteration of Lipid Composition by iPLA2-VIA Loss Affects Synaptic Functions. An increased proportion of shorter acyl chains in phospholipids affects the thickness and dynamics of biomembrane as well as the integrity of membrane-associated proteins (5). To determine the effects of altered lipid composition by iPLA2-VIA mutations on neuronal activity, we next examined the larval neuromuscular junctions (NMJs), which are well characterized as neuronal synaptic models. The synaptic morphology, including the number of docked vesicles, number of boutons, number of active zones in each bouton, and bouton size, was not changed by diPLA2-VIA loss (*SI Appendix*, Fig. S4 *A*, *B*, *D*, and *E*). Moreover, the overexpression of *hiPLA2-VIA* or *hC19orf12* or LA treatment had little effect on synaptic morphology (*SI Appendix*, Fig. S4 *A* and *B*). However, SV diameter in *diPLA2-VIA*$^{-/-}$ larvae was smaller than in *diPLA2-VIA*$^{+/+}$ larvae (Fig. 4 *A* and *B*). Consistent with the reduction in SV diameter in *diPLA2-VIA*$^{-/-}$ larvae, SV density near the active zones of *diPLA2-VIA*$^{-/-}$ flies was higher (*SI Appendix*, Fig. S4*C*). The SV phenotype was rescued by *hiPLA2-VIA*^{WT} or *dC19orf12*, but not *hiPLA2-VIA*^{A80T}, and the SV density near the active zones tended to change accordingly (*SI Appendix*, Fig. S4*C*).

Manipulation of acyl-chain composition by LA treatment also increased SV size (Fig. 4 *A* and *B*). Spontaneous neuronal activity, assessed by miniature excitatory junction potential (mEJP), was decreased in *diPLA2-VIA*$^{-/-}$ flies under 2 different ambient temperature conditions (22 and 30 °C), which was likely derived from the small SV phenotype because SV size as well as the number of boutons and active zones can affect mEJP amplitude (37). LA treatment and neuronal expression of *hiPLA2-VIA*^{WT}, but not *hiPLA2-VIA*^{A80T}, ameliorated the reduction in mEJP (Fig. 4 *C* and *D* and *SI Appendix*, Fig. S4*F*). hC19orf12^{WT}, but not MPAN-linked hC19orf12^{G69R}, also rescued the hypoactive mEJP phenotype of *diPLA2-VIA*$^{-/-}$ flies. Both mEJPs and EJPs tended to be lower in amplitude under a high temperature (30 °C) than a favorable temperature (22 °C; Fig. 4 *D* and *E*), and EJP amplitude as well as quantal content did not correlate with the alteration of lipid composition by gene manipulation and dietary treatment (Fig. 4*E* and *SI Appendix*, Fig. S4*G*). On the contrary, the paired-pulse ratios (PPRs) of *diPLA2-VIA*$^{-/-}$ flies and *diPLA2-VIA*$^{-/-}$ flies expressing *hiPLA2-VIA*^{A80T} were decreased by high temperature, perhaps due to the alteration in membrane fluidity (Fig. 4*E*).

Alteration of Lipid Composition by iPLA2-VIA Loss Accelerates α-Syn Fibril Formation. α-Synucleinopathy is a prominent feature of PD patients with *iPLA2-VIA* mutations and NBIA patients with *C19orf12* mutations (7, 28, 38). α-Syn repeatedly binds to and dissociates from the acidic phospholipid surface of SVs during the release and retrieval cycle of SVs (39). To explore the effects of altered lipid composition caused by iPLA2-VIA mutations on α-Syn stability, we neuronally expressed α-Syn in *diPLA2-VIA*$^{+/+}$ and *diPLA2-VIA*$^{-/-}$ flies. Aggregation of α-Syn, some of which was ubiquitin-positive, was observed to be intensive in *diPLA2-VIA*$^{-/-}$ DA neurons as well as other brain regions in 20-d-old adult flies, while few α-Syn-positive aggregations were detected in age-matched *iPLA2-VIA*$^{+/+}$ flies (Fig. 5 *A* and *B* and *SI Appendix*, Fig. S5*A*). Although ultrastructural analysis of adult brain tissues revealed that loss of iPLA2-VIA itself induced the appearance of abnormal organelle-derived membrane structures and electron-dense deposits, α-Syn–positive electron-dense deposits were frequently observed in the *diPLA2-VIA*$^{-/-}$ brain (*SI Appendix*, Fig. S5 *B* and *C*). Biochemical analysis indicated that most of these aggregates were sarkosyl-insoluble, suggesting that α-Syn was transformed from a native form to a pathogenic form (Fig. 5*C*) (40). Importantly, dietary LA treatment suppressed the aggregation and insolubilization of α-Syn (Fig. 5 *A*–*C*). Similar to LA treatment, the neuronal expression of *hiPLA2-VIA*^{WT} or *dC19orf12* ameliorated α-Syn aggregation, while *hiPLA2-VIA*^{A80T} failed to do so (Fig. 5 *D* and *E*).

To determine whether α-Syn aggregation generated in the *diPLA2-VIA*$^{-/-}$ brain exerts seeding activity on α-Syn fibril formation, we monitored the conversion of soluble α-Syn into amyloid fibrils by real-time quaking-induced conversion (RT-QUIC) using fly brain lysates expressing α-Syn (41, 42). The time required for thioflavin T (ThT) fluorescence to reach half of the fluorescence intensity was shorter under *diPLA2-VIA* loss, which was rescued by dietary LA treatment (Fig. 5 *F*, *Left*, and *SI Appendix*, Fig. S6*A*). In contrast, fly brain lysates without α-Syn expression did not have the seeding activity (*SI Appendix*, Fig. S6*B*). The slope values were not significantly different between genotypes and were comparable to those obtained from human brain tissues with LB pathology (*SI Appendix*, Fig. S6*C*), suggesting that fly α-Syn aggregates have properties similar to those from human brain (Fig. 5 *F*, *Right*). These observations strongly suggest that lipid alteration by *diPLA2-VIA* loss facilitates the pathogenic conformational change of α-Syn in fly brain.

Acyl-Chain Shortening Reduces the Affinity of α-Syn to Phospholipids. We next examined the effects of increased shorter acyl-chain
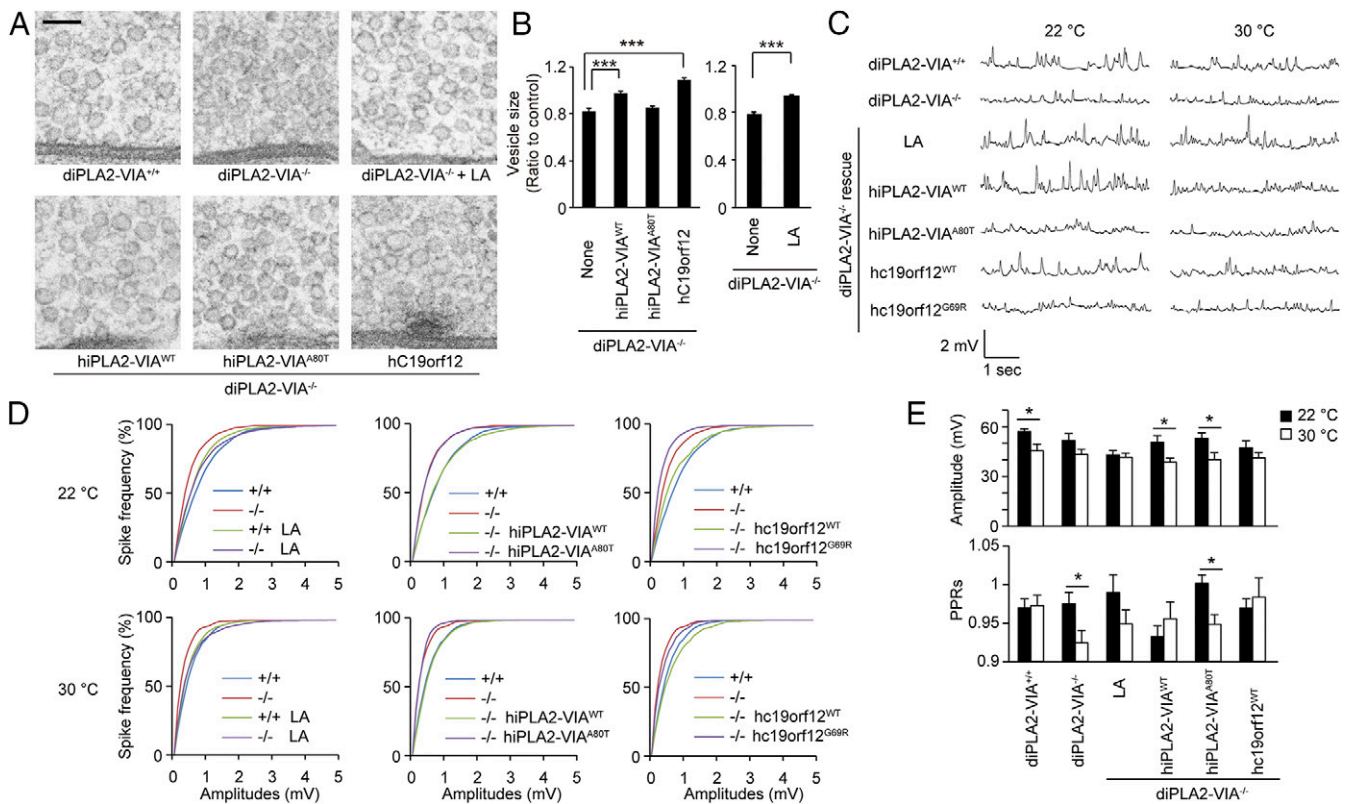
Fig. 4. Altered acyl-chain composition affects synaptic vesicle size. (A) Ultrastructure of the synaptic vesicles at the active zones in third-instar larval motor neurons with the indicated genotypes. (Scale bar, 100 nm.) (B) The ratio of synaptic vesicle diameter to $diPLA2$-$VI^{+/+}$ is graphed (mean ± SEM, n = 130 to 150 from 3 third-instar larvae; ***P < 0.0001 by 1-way ANOVA with the Tukey–Kramer test [Left] and by 2-tailed Student's t test [Right]). (C) Representative spontaneous mEJP traces in the third-instar larval NMJ at 22 and 30 °C. (D) Cumulative distribution of mEJP amplitude at 22 and 30 °C over 60 s (n = 7 to 11 third-instar larvae per genotype). (E) EJP amplitude evoked by 1.5 to 2 V electrical stimulation at 22 and 30 °C and paired-pulse ratio (PPR) as a ratio of EJP amplitudes to paired electrical stimulations (50-ms interval) at 22 and 30 °C (n = 7 to 9 third-instar larvae per genotype; *P < 0.05 by 2-tailed Student's t test).

phospholipids on the affinity of α-Syn to membrane. We prepared small unilamellar vesicles (SUVs) that contained 30% 1,2-dioleoyl-sn-glycero-3-phospho-L-serine (DOPS) and 70% PC with different acyl chains. A fluorescent probe to assess lipid packing, di-4-ANEPPDHQ, indicated that SUVs containing PC 16:0_14:0 showed loosened lipid packing compared to that of SUVs containing PC with C18 acyl chains (Fig. 6 A and B) (43, 44). SUVs containing PC 16:0_14:0 had a smaller diameter than those containing PC with C18 due to the higher curvature (Fig. 6C). Previous studies using liposomes have shown that the N-terminal amphiphilic helix of α-Syn recognizes packing defects and acidic head groups of phospholipids through its hydrophobic side and basic charged regions, respectively (45–47). Because α-Syn presents at presynapses at ∼20 μM, we incubated the above SUVs (500 μM) with 5 μM recombinant α-Syn (48). Surprisingly, native PAGE indicated that α-Syn lost its affinity to SUVs containing PC 16:0_14:0, while it bound by its N-terminal region to SUVs containing PC with C18 acyl chains (Fig. 6D and *SI Appendix*, Fig. S6D). Lack of interaction between the PC 16:0_14:0 SUVs and α-Syn was also supported by liposome surface ζ-potential analysis, in which α-Syn affected the ζ potential of PC 16:0_14:0 SUVs to a lesser degree (Fig. 6E).

Discussion

In this study, using *Drosophila iPLA2-VIA* mutant models, we make 3 contributions to the understanding of the etiology of PD and NBIA. First, lack of iPLA2-VIA activity results in the shortening of phospholipid acyl chains, which evokes ER stress and affects neuronal activity. Second, the ectopic expression of

MPAN-associated C19orf12 rescues the neuronal phenotypes caused by iPLA2-VIA loss. Third, α-Syn aggregation is facilitated by phospholipids with shorter acyl chains (Fig. 7).

The structural diversity of lipids influences their geometry, curvature, fluidity, thickness, surface charge, and lipid packing. iPLA2-VIA, which converts phospholipids into inverse cone-shaped lysophospholipids on the plasma membrane, releasing FAs in the process, plays a crucial role in regulating the synaptic transmission and electrical properties in the neuronal and glial cells (49, 50). PLA₂ activity contributes to SV formation at synaptic terminals, as demonstrated by previous studies that venom containing PLA₂ neurotoxins promotes SV exocytosis and inhibits synaptic endocytosis (51, 52). Our study revealed that the phospholipid acyl chains get progressively shorter in the $diPLA2$-$VIA^{-/-}$ flies (*SI Appendix*, Fig. S2E). An increased proportion of shorter acyl chains caused by iPLA2-VIA loss leads to higher membrane curvature. Consistent with this finding, we observed reduced SV size and mEJPs in $diPLA2$-$VIA^{-/-}$, and $diPLA2$-$VIA^{-/-}$;$hiPLA2$-VIA^{A80T} larval NMJs (Fig. 4 A–D), whereas EJPs of $diPLA2$-$VIA^{-/-}$ and $diPLA2$-$VIA^{-/-}$;$hiPLA2$-VIA^{A80T} larvae were largely intact despite the obvious seizure-paralysis phenotype at an early adult stage. The seizure-paralysis phenotype has been reported in flies harboring mutations in mitochondrial proteins or ion channels and genes associated with lipid metabolism, which might be due to the defects in energy supply and altered channel activities on the biomembrane (15). Thus, age-dependent alterations in the synaptic membrane properties and mitochondrial dysfunction might synergistically contribute to the seizure-paralysis phenotype and early motor defects, although our $diPLA2$-$VIA^{-/-}$ flies did not
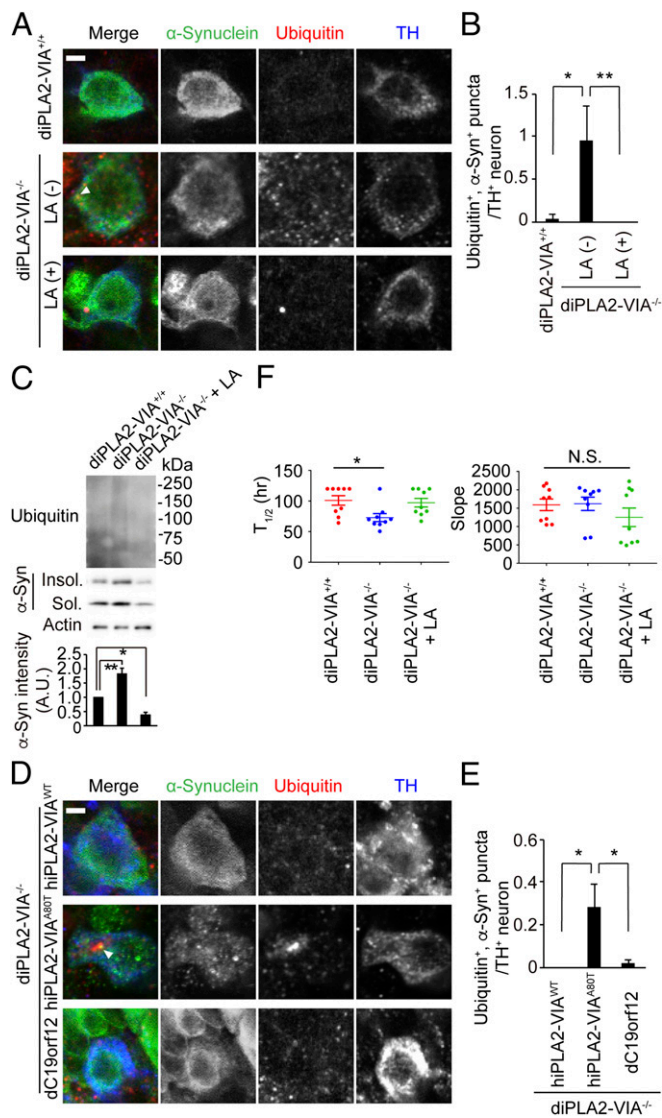
Fig. 5. Alteration of phospholipid composition by *diPLA2-VIA* loss promotes α-Syn aggregation. (*A–C*) α-Syn accumulation by *diPLA2-VIA* loss is relieved by the LA diet. (*A*) Brain tissues from 15-d-old flies were stained with the indicated antibodies. An arrowhead indicates ubiquitin- and α-Syn–positive punctum. (Scale bar, 2 μm.) (*B*) Ubiquitin- and α-Syn–positive puncta in TH-positive neurons are graphed (*n* = 10 to 15 neurons from 6 flies at 15 d old per sample; *P < 0.05 and **P < 0.01 by 1-way ANOVA with the Tukey–Kramer test). (*C*) Sarkosyl-soluble and -insoluble fractions from brain tissues from 20-d-old flies were analyzed by Western blot. The band intensities of α-Syn normalized to those of actin are graphed (*n* = 4; *P < 0.05 and **P < 0.01 by Dunnett's test). (*D* and *E*) α-Syn accumulation caused by *diPLA2-VIA* loss is suppressed by *hiPLA2-VIA* or *dC19orf12*. (*D*) Brain tissues from 15-d-old flies were stained with the indicated antibodies. An arrowhead indicates ubiquitin- and α-Syn–positive punctum. (Scale bar, 2 μm.) (*E*) Ubiquitin- and α-Syn–positive puncta in TH-positive neurons are graphed (*n* = 10 to 15 neurons from 6 flies at 15 d old per sample; *P < 0.05 by 1-way ANOVA with the Tukey–Kramer test). (*F*) *diPLA2-VIA* loss promotes the seeding activity of α-Syn. Brain lysates prepared from 15-d-old flies neuronally expressing α-Syn were subjected to RT-QUIC. Graphs indicate the time when TdT fluorescence reached an intensity of 165,000 RFU (*Left*, $t_{1/2}$) and the slope obtained by differential processing of plot curves (*Right*), respectively. When TdT fluorescence did not reach 165,000 RFU before 120 h, the value of $t_{1/2}$ was defined as 120 (*n* = 3 replicates from 3 flies per sample; *P < 0.05 by 1-way ANOVA with the Tukey–Kramer test). N.S., not significant; RFU, relative fluorescence units.

exhibit obvious mitochondrial defects. Morphological defects in the ER and XBP1 activation at the developmental stages were observed at least in the salivary grands, and sporadic XBP1 activation was also detected in the aged brain of *diPLA2-VIA*$^{-/-}$ flies, suggesting that the disruption of membrane lipid equilibrium due to iPLA2-VIA loss leads to chronic ER stress, resulting in widespread neurodegeneration including DA neuron death. Chronic ER stress would also compromise the secretion of neuropeptides such as PDF, a vasoactive intestinal peptide-like neuropeptide in flies via the ER (36). While sleep disturbance is one of the prodromal symptoms associated with PD (1), age-dependent defects in circadian and sleep pattern of *diPLA2-VIA*$^{-/-}$ flies could be explained by the dysregulated release of dopamine and PDF as well as by the disconnection of neural circuits (*SI Appendix*, Fig. S1D) (19, 36).

Functions of iPAL2-VIA related to lipid metabolism have been proposed in many in vivo studies. These functions include membrane remodeling (14, 25), DHA and ARA metabolism (25, 53, 54), and lysophospholipid production and the subsequent activation of store-operated Ca^{2+} entry (55). Our unexpected result of acyl-chain shortening raises the possibility that iPLA2-VIA preferentially hydrolyzes 14:0 phospholipids, which could eventually affect the metabolism of other classes of lipids and maintain the membrane lipid composition and ER homeostasis (33, 56). A recent study has reported that diPLA2-VIA loss does not alter phospholipid headgroup composition, which is consistent with our findings (*SI Appendix*, Fig. S2D), but instead promotes sphingolipid accumulation due to compromised retromer functions, leading to further dysfunction of the retromer complex and concomitant lysosomal stress (30). Although the phospholipid acyl-chain composition was not analyzed in that study, most of the sphingolipid molecular species that were altered in the *diPLA2-VIA*–deficient flies had a 14:0 acyl chain (30). In mammals, 16:0-lysoPC is preferentially produced by iPLA2-VIA in activated macrophages; however, there is a lack of information on 14:0-lysoPC (57). These observations may suggest that iPLA2-VIA recognizes 14:0 or 16:0 phospholipids at the *sn-1* position.

Lipid oxidation is exacerbated in *diPLA2-VIA*$^{-/-}$ flies, which reveals the role of iPLA2-VIA in removing oxidized acyl chains (14). Although our finding does not exclude the antioxidative role of iPLA2-VIA in the biomembrane, the null effects of α-tocopherol on motor behavior, seizure phenotype, and DA neuron loss indicate that lipid oxidation is not a direct cause of PLAN-linked neurodegeneration. In iPLA2-VIA–knockout mice, there are inconsistent results regarding changes in brain lipids, which may be due to differences in experimental methods and the lipid and FA species investigated (25, 54). Currently, it appears to be difficult to evaluate whether our findings regarding lipid changes in *Drosophila melanogaster*, which has few longer acyl-chain lipids such as DHA- and ARA-containing phospholipids, reflect the events observed in mouse models (58). Further studies will be required to determine the molecular mechanism of acyl-chain shortening and retromer regulation by iPLA2-VIA, especially in mammalian models.

The regulation of MAM by C19orf12 and the up-regulation of C19orf12 during adipocyte differentiation imply C19orf12 involvement in lipid metabolism (35, 59). The rescue of *iPLA2-VIA* neuronal phenotypes by C19orf12 expression provides molecular insight into the common underlying pathogenesis of PLAN and MPAN. Loss of iPLA2-VIA prominently alters ER morphology in salivary gland cells, and this change may also affect the integrity of the MAM structure, through which PS transported from the ER is converted to PE by mitochondrial PS decarboxylase (60). Although our phospholipid measurement method did not detect PS with high sensitivity, the abundance of PE was not changed by *iPLA2-VIA* loss, suggesting that PE synthesis is largely dependent on, or is compensatorily bypassed through, the
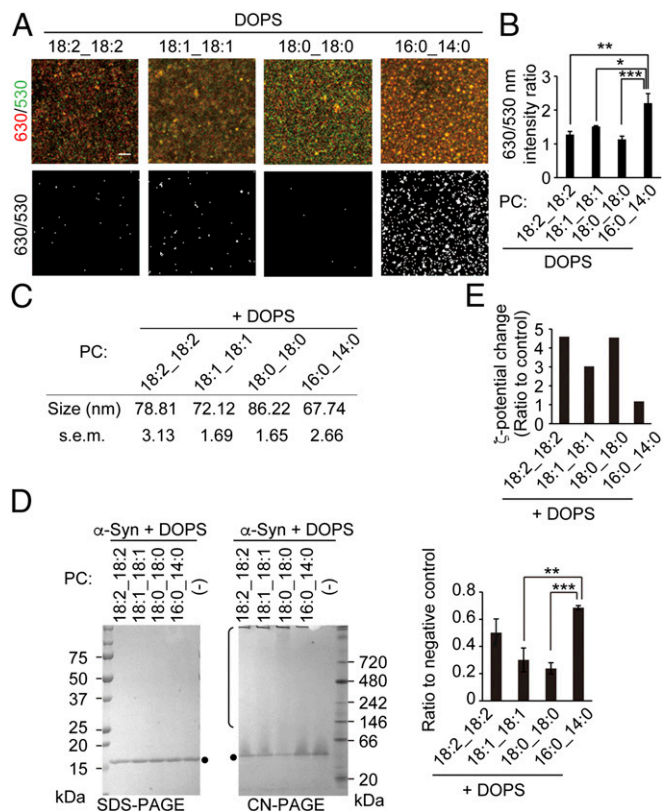
MEDICAL SCIENCES

Fig. 6. A shorter acyl-chain composition weakens α-Syn association with liposomes. (*A* and *B*) Lipid packing status of SUVs. (*A*) SUVs containing 30% DOPS and 70% of the indicated phospholipids were incubated with 250 nM di-4-ANEPPDHQ, and the fluorescence intensities at 630 and 530 nm were imaged (*Upper*). The 630-nm signal divided by the thresholded 530-nm signal intensity is also shown (*Lower*). (Scale bar, 2 μm.) (*B*) The 630/530-nm intensity ratios are graphed ($n = 3$ to 4; *$P < 0.05$, **$P < 0.01$, and ***$P < 0.005$ by 1-way ANOVA with the Tukey–Kramer test). (*C*) Diameter (in nanometers) of SUVs containing 30% DOPS and 70% of the indicated phospholipids (mean ± SEM; 3 trials). (*D*) α-Syn does not bind to SUVs containing shorter acyl chains. Five micromolar recombinant α-Syn incubated with 500 μM SUV as prepared in *A–C* for 10 min was separated by clear-native PAGE (CN-PAGE) or SDS/PAGE. Dots and open bracket indicate a monomer form of α-Syn and slower-migrating forms of α-Syn due to the interaction with SUV, respectively. Graph represents the ratios of α-Syn monomer signals to a control without SUV on CN-PAGE, normalized to α-Syn signals that appeared on SDS/PAGE as inputs ($n = 3$; **$P < 0.01$ and ***$P < 0.001$ by Dunnett's test). (*E*) ζ Potentials of SUVs with recombinant α-Syn are indicated as a ratio to that of control liposomes without proteins.

Kennedy pathway. Nevertheless, the rescue of ER stress in *diPLA2-VIA*$^{-/-}$ flies by C19orf12 raises the possibility that the enhancement of MAM integrity alleviates membrane lipid disequilibrium.

Similar to postmortem studies in INAD and PARK14, *diPLA2-VIA*$^{-/-}$ flies exhibited ubiquitinated α-Syn accumulation in DA neurons as well as other types of neurons (Fig. 5 and *SI Appendix*, Fig. S5), a phenomenon that was rescued by C19orf12; C19orf12 mutations also lead to α-Syn accumulation and subsequent LB formation (28). The interaction between α-Syn and lipids modulates α-Syn fibril formation in different ways, and there have been controversial observations of the pathological roles of the lipid membrane in terms of α-Syn aggregation (2, 61–63). Our fly models suggest that changes in the acyl-chain composition of phospholipids are more critical for α-Syn aggregation than changes in the head group. Although we cannot exclude the possibility that decreased unsaturation of acyl chains contributed to neurodegeneration in our *Drosophila* models, the results of

the liposome assay indicate that the status of lipid packing produced by the geometry of acyl chains in the lipid bilayers affects α-Syn stability. Increased shorter acyl chains would lead to higher membrane curvature and larger packing defects, whereas the polyunsaturation of acyl chains shallows the hydrophobic groove (64). While lipid-packing defects facilitate α-Syn insertion into the membrane (46, 65), α-Syn loses its affinity to SUVs containing PC with shorter acyl chains (Fig. 6). This inconsistency may derive from differences in the depth of the hydrophobic groove and the state of the gel/liquid crystalline phases generated by different FA compositions (49, 66). Nevertheless, the finding that α-Syn lacking 30 N-terminal residues (ΔN30) has greater in vivo seeding activity than full-length α-Syn supports our idea (67). The N-terminal helical segment of α-Syn, composed of 25 residues, has been demonstrated to function as a membrane anchor, and ΔN30 failed to bind to liposomes in our assay (*SI Appendix*, Fig. S6D) (68). Considering the previous related studies, our data suggest that nonmembrane-bound α-Syn carries a risk of aggregation and/or that the association of α-Syn with membranes that contain shorter acyl chains contributes to its aggregation (69).

The observation that the correction of phospholipid composition by dietary LA treatment alleviates the ER stress and the neuronal phenotypes of *diPLA2-VIA*$^{-/-}$ flies strongly suggests that acyl-chain shortening of phospholipids in the brain could be the major pathogenic mechanism underlying PLAN-linked neurodegeneration (*SI Appendix*, Fig. S7). The administration of a diet containing lower amounts of polyunsaturated phospholipids causes a decrease in the speed and sensitivity of phototransduction in *Drosophila* (24). In the mammalian brain, PUFAs including LA are supplied through the blood, indicating that altered dietary intake of PUFAs could affect neuronal functions (70). The relationship between dietary intake of FAs and PD has been investigated. Cohort studies showed that dietary intake of vitamin E had little effect on PD risk (71), while intake of unsaturated FAs reduced PD risk (72). In contrast, saturated fat and ω-6 PUFAs might be associated with PD risk (73, 74). Although beneficial FAs in humans corresponding to LA in *Drosophila* need to be determined, our study indicates that the dietary manipulation of FAs is a promising method to control risks for PD and related disorders.
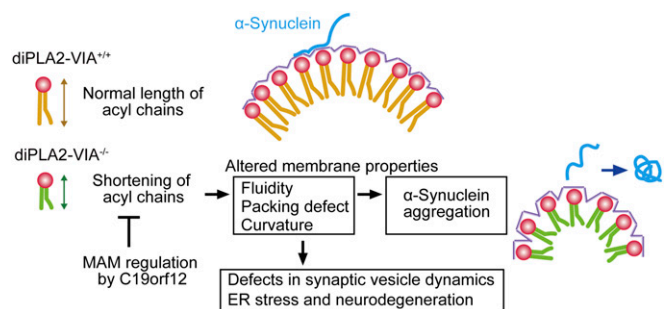

Fig. 7. Working hypothesis. Loss of iPLA2-VIA causes the shortening of phospholipid acyl chains in the brain, which alters membrane fluidity, lipid packing, and curvature. α-Syn affinity to the synaptic membrane is weakened by altered phospholipid properties, leading to α-Syn aggregation. These altered membrane properties also induce ER stress, affect the dynamics of SVs, and provoke abnormal neurotransmission, which manifests as the bang-sensitivity phenotype. Correction of the membrane composition by dietary intake of FAs or enhanced MAM integrity by C19orf12 rescues neurodegeneration and α-Syn aggregation.

Materials and Methods

Extended experimental procedures are described in *SI Appendix, SI Materials and Methods*. All vectors, *Drosophila* stocks, and primary antibodies are listed in *SI Appendix*, Tables S1–S3.

Fly Stocks. Fly culture and crosses were performed on standard fly food containing yeast, cornmeal, and molasses, and the flies were raised at 25 °C. Complementary DNAs (cDNAs) for *hiPLA2-VIA*, *hc19orf12*, and their disease-associated mutants were subcloned into the *pUAST attB* vector using the In-fusion HD Cloning Kit (Takara Bio) with the following primer pairs: 5′-GGCCGCG GCTCGAGGGTACCATGCAGTTCTTTGGCCGCCTGGTCAATAC-3′, 5′-AAAGAT CCTCTAGAGGTACCTCAGGGTGAGAGCAGCAGCAGCTGGA-3′ for *hiPLA2-VIA*; and 5′-AGGGAATTGGGAATTATGGAGAGGCTGAAGTCAC-3′, 5′-ATCTGT-TAACGAATTCTAGTCATCATACTGGATCT-3′ for *hc19orf12*. The transgenic lines were generated on *y¹w¹¹¹⁸;pBac{y⁺-attP-3B}VK00037* (Bloomington stock 9752) background (BestGene). *pUAS-ER-mAG1* was subcloned from pER-mAG1 (MBL, AM-V0202M), and transgenic lines were generated on the *w¹¹¹⁸* background (BestGene). All other fly stocks and GAL4 lines used in this study were obtained from the Bloomington *Drosophila* Stock Center and Kyoto Stock Center. *UAS-α-Synuclein^{LP2}* (75) and *UAS-mito-TdTomato* (76) were gifts from L. J. Pallanck, University of Washington School of Medicine, and T. Uemura, Kyoto University Graduate School of Biostudies, respectively. Stocks were backcrossed to the *w¹¹¹⁸* wild-type background for 6 generations.

Generation of *diPLA2-VIA* Null Allele. The *diPLA2-VIA* null allele was generated by CRISPR-Cas9 technology using tandem guide RNA plasmids (pCFD4) and a fly line expressing Cas9 during oogenesis (Bloomington stock 54591). Two protospacers corresponding to sequences of dIPLA2-VIA were cloned into Bbs I-digested pCFD4 with the In-fusion HD Cloning Kit with the primer pair 5′-TATATAGGAAAGATATCCGGGTGAACTTCGTCGGGCAGCAACGGATA GCGTTTTAGAGCTAGAAATAGCAAG-3′, 5′-ATTTTAACTTGCTATTTCTAGCTC TAAAACTCTACTGGAGATGGTGGCTCGACGTTAAATTGAAAATAGGTC-3′. To avoid potential off-target mutations generated by Cas9, the *diPLA2-VIA* null allele was backcrossed to the *w¹¹¹⁸* background for 6 generations, and *w¹¹¹⁸* was used as a control allele. The sequences of the forward and reverse primers for genotyping were as follows:

iPLA2-VIA genomic Fw, 5′-CGGTGACATCGCTAATAAAGCTGC; iPLA2-VIA genomic Rev, 5′-GCGGTCTAAATCCGTCTTGCATG.

Quantitative Reverse Transcription-PCR. Full details of quantitative reverse transcription PCR are provided in *SI Appendix, SI Materials and Methods*.

Imaging and EM Analysis. Full details of imaging and EM analysis are provided in *SI Appendix, SI Materials and Methods*.

Administration of FAs and α-Tocopherol. Flies were reared on either a plain diet (Formula 4–24 Plain *Drosophila* Medium; Carolina Biological Supply); a diet with the addition of one of the following FAs at 5 μL/mL unless otherwise indicated: linoleic acid (L1012; Sigma-Aldrich), stearic acid (198-12481; Wako), or myristic acid (134-03435; Wako); or a diet with 25 IU/mL α-tocopherol (207-01792; Wako) as reported previously (24, 77, 78).

Lipid Extraction and Lipids Analysis by Electrospray Ionization Mass Spectrometry (ESI-MS). Samples for ESI-MS of lipids were prepared and analyzed as described previously (79). In brief, brain tissues of flies reared on a plain diet (Formula 4–24 Plain *Drosophila* Medium) or a diet with the addition of 5 μL/mL LA were soaked in 200 μL of 50 mM Tris·HCl (pH 7.4) and then homogenized on ice for 1 min. Lipids were extracted from the homogenates by the Bligh and Dyer method (79). Analysis was performed using a quadrupole-linear ion-trap hybrid mass spectrometer (4000Q-TRAP; Sciex) equipped with a liquid chromatograph (Nexera X2 system; Shimadzu). As an internal standard, 500 pmol of *d*5-labeled eicosapentaenoic acid was added to each sample. Samples injected by an autosampler were separated using a step gradient with mobile phase A (acetonitrile/methanol/water = 1:1:1 [vol/vol/v] containing 5 μM phosphoric acid and 1 mM ammonium formate) and mobile phase B (2-propanol containing 5 μM phosphoric acid and 1 mM ammonium formate) at a flow rate of 0.2 mL/min at 50 °C. Identification was conducted using multiple reaction monitoring transition and retention times, and quantification was performed based on the peak area of the multiple reaction monitoring transition and calibration curve obtained with an authentic standard for each compound, as described previously (79).

Biochemical Analysis and α-Syn Fractionation. Full details of biochemical analysis and α-Syn fractionation are provided in *SI Appendix, SI Materials and Methods*.

RT-QUIC. Recombinant human α-Syn protein was purified from *Escherichia coli* BL21 harboring pRK172-α-Syn (Y136-TAT) as previously reported (80). A female fly head homogenized in 20 μL of ice-cold phosphate buffered saline (PBS) supplemented with 1/100 protease inhibitor mixture (Nacalai) in 1.5-mL tubes was sonicated for 3 min on ice using a sonicator (Branson Sonifier 250, micro tip power 3 to 4, 30 s sonication/30 s pause, 3 times). After centrifugation at $2,000 \times g$ for 2 min at 4 °C to remove debris, the supernatant diluted with PBS at 1:10 was used as a fly brain sample. The RT-QUIC assay was performed according to a reported protocol (41). Briefly, the RT-QUIC reaction buffer (RB) was composed of 100 mM phosphate buffer (pH 8.2), 10 μM ThT, and 0.1 mg/mL recombinant α-Syn. Each well of a black 96-well plate with a clear bottom (Nalgene Nunc) contained 95 μL of RB and 37 ± 3 mg of 0.5-mm zirconium/silica beads (Thistle Scientific). Reactions were seeded with 5 μL of fly brain samples to a final reaction volume of 100 μL. The plates were sealed with plate sealer film (Greiner Bio-One) and incubated in a FLUOstar OPTIMA microplate reader (BMG Labtech) at 30 °C for 120 h with intermittent shaking cycles: double-orbital with 1 min of shaking at 200 rpm followed by 14 min of rest. ThT fluorescence measurements (450 nm excitation and 480 nm emission) were taken every 15 min.

Liposome Assay. DLPC, DOPC, DSPC, PC16:0_14:0, and DOPS were purchased from Avanti Polar Lipids. DLPC/DOPS (7:3), DOPC/DOPS (7:3), DSPC/DOPS (7:3), and PC16:0_14:0/DOPS (7:3) in chloroform were dried by a nitrogen evaporator. The lipids resuspended in 1 mL of 50 mM NaCl were prepared by sequential extrusion through 0.1-μm and 0.05-μm filters by using a hand extruder (Avanti Polar Lipids). The suspension of 50 μM liposomes with or without recombinant 5 μM α-Syn vortexed briefly was incubated for 10 min at RT, and liposome size and ζ potentials were measured using a Zetasizer-NanoZSP (Malvern Instruments). For CN-PAGE, 5 μM α-Syn with or without 500 μM liposomes in TBS (pH 7.4) vortexed briefly was incubated for 10 min at RT. The samples were mixed with 4× CN-PAGE sample buffer and separated on a 4 to 16% Bis-Tris gel (Thermo Fisher Scientific). NativeMark Unstained Protein Standard (Thermo Fisher Scientific) was used to estimate molecular mass. The gel was run at 100 V for 100 min and was stained with One-step Coomassie brilliant blue staining reagent (Bio Craft). To assess packing defects, 100 μM liposomes incubated with 250 nM di-4-ANEPPDHQ dye at RT for 30 min were analyzed using confocal microscopy (LSM880; Zeiss).

***Drosophila* Behavior Assays and Survival Assay.** Full details of *Drosophila* behavior assays and survival assay are provided in *SI Appendix, SI Materials and Methods*.

Electrophysiology. Third-instar larvae were dissected in HL-3, and mEJPs from NMJs were recorded using an electrophysiological setup equipped with an Eclipse FN1 microscope (Nikon), a Multiclamp 700B amplifier (Molecular Devices), and a Digidata 1550A data acquisition system (Molecular Devices). Dissected larvae were incubated in HL-3 containing 2.5 mM (for EJP) or 0.375 mM (for mEJP) Ca²⁺, and a recording electrode filled with 3 M KCl was inserted into muscle 6 of the A3 segment containing NMJs. All data were analyzed using Mini-Analysis software (Synaptosoft). Quantal content was calculated as the mean EJP amplitude divided by the mean mEJP amplitude, as previously described (37).

Statistical Analyses. Error bars in graphs represent the mean ± SEM. The exact sample size (e.g., the number of flies, brains, or neurons) of each experiment is provided in the relevant figures. A 2-tailed Student's *t* test or 1-way repeated-measures ANOVA was used to detect significant differences between 2 or among multiple groups, respectively, unless otherwise indicated. If a significant result was detected using ANOVA ($P < 0.05$), the mean values of the control and the specific test group were analyzed using the Tukey–Kramer test. Dunnett's test was used to detect significant differences between 2 specific groups or among multiple groups of interest. Data distribution was assumed to be normal, but this was not formally tested. Data collection and analysis were performed by researchers (A.M., T.I., K.S.-F., H.M., S.S., and A.O.) blinded to the conditions in key experiments (Figs. 1*E*, 2*D*, 3 *D* and *F*, 5 *B*, *E*, and *F* and *SI Appendix*, Figs. S1G, S2 *E*, *F*, and *J*, S3J, and S6 *A* and *B*).

MEDICAL SCIENCES

1. L. V. Kalia, A. E. Lang, Parkinson's disease. *Lancet* **386**, 896–912 (2015).
2. P. K. Auluck, G. Caraveo, S. Lindquist, α-Synuclein: Membrane interactions and toxicity in Parkinson's disease. *Annu. Rev. Cell Dev. Biol.* **26**, 211–233 (2010).
3. C. C. Jao, B. G. Hegde, J. Chen, I. S. Haworth, R. Langen, Structure of membrane-bound alpha-synuclein from site-directed spin labeling and computational refinement. *Proc. Natl. Acad. Sci. U.S.A.* **105**, 19666–19671 (2008).
4. K. Bozek *et al*., Organization and evolution of brain lipidome revealed by large-scale analysis of human, chimpanzee, macaque, and mouse tissues. *Neuron* **85**, 695–702 (2015).
5. B. Antonny, S. Vanni, H. Shindou, T. Ferreira, From zero to six double bonds: Phospholipid unsaturation and organelle function. *Trends Cell Biol.* **25**, 427–436 (2015).
6. J. E. Burke, E. A. Dennis, Phospholipase A2 biochemistry. *Cardiovasc. Drugs Ther.* **23**, 49–59 (2009).
7. A. Gregory *et al*., Neurodegeneration associated with genetic defects in phospholipase A(2). *Neurology* **71**, 1402–1409 (2008).
8. C. Paisán-Ruiz *et al*., Widespread Lewy body and tau accumulation in childhood and adult onset dystonia-parkinsonism cases with PLA2G6 mutations. *Neurobiol. Aging* **33**, 814–823 (2012).
9. S. Levi, D. Finazzi, Neurodegeneration with brain iron accumulation: Update on pathogenic mechanisms. *Front. Pharmacol.* **5**, 99 (2014).
10. N. V. Morgan *et al*., PLA2G6, encoding a phospholipase A2, is mutated in neurodegenerative disorders with high brain iron. *Nat. Genet.* **38**, 752–754 (2006).
11. C. C. Chiu *et al*., PARK14 PLA2G6 mutants are defective in preventing rotenone-induced mitochondrial dysfunction, ROS generation and activation of mitochondrial apoptotic pathway. *Oncotarget* **8**, 79046–79060 (2017).
12. L. A. Engel, Z. Jing, D. E. O'Brien, M. Sun, P. T. Kotzbauer, Catalytic function of PLA2G6 is impaired by mutations associated with infantile neuroaxonal dystrophy but not dystonia-parkinsonism. *PLoS One* **5**, e12897 (2010).
13. I. Kudo, M. Murakami, Phospholipase A2 enzymes. *Prostaglandins Other Lipid Mediat.* **68–69**, 3–58 (2002).
14. K. J. Kinghorn *et al*., Loss of PLA2G6 leads to elevated mitochondrial lipid peroxidation and mitochondrial dysfunction. *Brain* **138**, 1801–1816 (2015).
15. M. G. Burg, C. F. Wu, Mechanical and temperature stressor-induced seizure-and-paralysis behaviors in Drosophila bang-sensitive mutants. *J. Neurogenet.* **26**, 189–197 (2012).
16. P. Agarwal *et al*., Imaging striatal dopaminergic function in phospholipase A2 group VI-related parkinsonism. *Mov. Disord.* **27**, 1698–1699 (2012).
17. A. Freeman *et al*., Sleep fragmentation and motor restlessness in a Drosophila model of Restless Legs Syndrome. *Curr. Biol.* **22**, 1142–1148 (2012).
18. M. B. Gajula Balija, C. Griesinger, A. Herzig, M. Zweckstetter, H. Jäckle, Pre-fibrillar α-synuclein mutants cause Parkinson's disease-like non-motor symptoms in Drosophila. *PLoS One* **6**, e24701 (2011).
19. T. Ueno *et al*., Identification of a dopamine pathway that regulates sleep and arousal in Drosophila. *Nat. Neurosci.* **15**, 1516–1523 (2012).
20. A. I. de Kroon, P. J. Rijken, C. H. De Smet, Checks and balances in membrane phospholipid class and acyl chain homeostasis, the yeast perspective. *Prog. Lipid Res.* **52**, 374–394 (2013).
21. R. A. Bowen, M. T. Clandinin, Dietary low linolenic acid compared with docosahexaenoic acid alter synaptic plasma membrane phospholipid fatty acid composition and sodium-potassium ATPase kinetics in developing rats. *J. Neurochem.* **83**, 764–774 (2002).
22. M. T. Clandinin *et al*., Assessment of the efficacious dose of arachidonic and docosahexaenoic acids in preterm infant formulas: Fatty acid composition of erythrocyte membrane lipids. *Pediatr. Res.* **42**, 819–825 (1997).
23. B. Levant, M. K. Ozias, S. E. Carlson, Specific brain regions of female rats are differentially depleted of docosahexaenoic acid by reproductive activity and an (n-3) fatty acid-deficient diet. *J. Nutr.* **137**, 130–134 (2007).
24. A. S. Randall *et al*., Speed and sensitivity of phototransduction in Drosophila depend on degree of saturation of membrane phospholipids. *J. Neurosci.* **35**, 2731–2746 (2015).
25. G. Beck *et al*., Neuroaxonal dystrophy in calcium-independent phospholipase A2β deficiency results from insufficient remodeling and degeneration of mitochondrial and presynaptic membranes. *J. Neurosci.* **31**, 11411–11420 (2011).
26. Y. Imai *et al*., The loss of PGAM5 suppresses the mitochondrial degeneration caused by inactivation of PINK1 in Drosophila. *PLoS Genet.* **6**, e1001229 (2010).
27. H. Meng *et al*., Loss of Parkinson's disease-associated protein CHCHD2 affects mitochondrial crista structure and destabilizes cytochrome c. *Nat. Commun.* **8**, 15500 (2017).
28. P. Hogarth *et al*., New NBIA subtype: Genetic, clinical, pathologic, and radiographic features of MPAN. *Neurology* **80**, 268–275 (2013).
29. A. Iuso *et al*., Impairment of Drosophila orthologs of the human orphan protein C19orf12 induces bang sensitivity and neurodegeneration. *PLoS One* **9**, e89439 (2014).
30. G. Lin *et al*., Phospholipase PLA2G6, a parkinsonism-associated gene, affects Vps26 and Vps35, retromer function, and ceramide levels, similar to α-Synuclein gain. *Cell Metab.* **28**, 605–618.e6 (2018).
31. X. Lei, S. Zhang, A. Bohrer, S. Ramanadham, Calcium-independent phospholipase A2 (iPLA2 beta)-mediated ceramide generation plays a key role in the cross-talk between the endoplasmic reticulum (ER) and mitochondria during ER stress-induced insulin-secreting cell apoptosis. *J. Biol. Chem.* **283**, 34819–34832 (2008).
32. K. R. Malley *et al*., The structure of iPLA₂β reveals dimeric active sites and suggests mechanisms of regulation and localization. *Nat. Commun.* **9**, 765 (2018).
33. K. Halbleib *et al*., Activation of the unfolded protein response by lipid bilayer stress. *Mol. Cell.* **67**, 673–684.e8 (2017).
34. N. Amin-Wetzel *et al*., A J-protein Co-chaperone recruits BiP to monomerize IRE1 and repress the unfolded protein response. *Cell* **171**, 1625–1637.e13 (2017).
35. P. Venco *et al*., Mutations of C19orf12, coding for a transmembrane glycine zipper containing mitochondrial protein, cause mis-localization of the protein, inability to respond to oxidative stress and increased mitochondrial Ca²⁺. *Front. Genet.* **6**, 185 (2015).
36. J. S. Valadas *et al*., ER lipid defects in neuropeptidergic neurons impair sleep patterns in Parkinson's disease. *Neuron* **98**, 1155–1169.e6 (2018).
37. T. Inoshita *et al*., Vps35 in cooperation with LRRK2 regulates synaptic vesicle endocytosis through the endosomal pathway in Drosophila. *Hum. Mol. Genet.* **26**, 2933–2948 (2017).
38. Y. Miki *et al*., Neuropathology of PARK14 is identical to idiopathic Parkinson's disease. *Mov. Disord.* **32**, 799–800 (2017).
39. J. Burré, M. Sharma, T. C. Südhof, α-Synuclein assembles into higher-order multimers upon membrane binding to promote SNARE complex formation. *Proc. Natl. Acad. Sci. U.S.A.* **111**, E4274–E4283 (2014).
40. M. Masuda-Suzukake *et al*., Prion-like spreading of pathological α-synuclein in brain. *Brain* **136**, 1128–1138 (2013).
41. G. Fairfoul *et al*., Alpha-synuclein RT-QuIC in the CSF of patients with alpha-synucleinopathies. *Ann. Clin. Transl. Neurol.* **3**, 812–818 (2016).
42. K. Sano *et al*., Prion-like seeding of misfolded α-Synuclein in the brains of dementia with Lewy body patients in RT-QUIC. *Mol. Neurobiol.* **55**, 3916–3930 (2018).
43. M. Amaro, F. Reina, M. Hof, C. Eggeling, E. Sezgin, Laurdan and Di-4-ANEPPDHQ probe different properties of the membrane. *J. Phys. D Appl. Phys.* **50**, 134004 (2017).
44. D. M. Owen, C. Rentero, A. Magenau, A. Abu-Siniyeh, K. Gaus, Quantitative imaging of membrane lipid order in cells and organisms. *Nat. Protoc.* **7**, 24–35 (2011).
45. W. S. Davidson, A. Jonas, D. F. Clayton, J. M. George, Stabilization of alpha-synuclein secondary structure upon binding to synthetic membranes. *J. Biol. Chem.* **273**, 9443–9449 (1998).
46. M. M. Ouberai *et al*., α-Synuclein senses lipid packing defects and induces lateral expansion of lipids leading to membrane remodeling. *J. Biol. Chem.* **288**, 20883–20895 (2013).
47. S. S. Chong, S. G. Taneva, J. M. Lee, R. B. Cornell, The curvature sensitivity of a membrane-binding amphipathic helix can be modulated by the charge on a flanking region. *Biochemistry* **53**, 450–461 (2014).
48. B. G. Wilhelm *et al*., Composition of isolated synaptic boutons reveals the amounts of vesicle trafficking proteins. *Science* **344**, 1023–1028 (2014).
49. E. Lauwers, R. Goodchild, P. Verstreken, Membrane lipids in presynaptic function and disease. *Neuron* **90**, 11–25 (2016).
50. D. Piomelli, G. Astarita, R. Rapaka, A neuroscientist's guide to lipidomics. *Nat. Rev. Neurosci.* **8**, 743–754 (2007).
51. C. Montecucco, O. Rossetto, How do presynaptic PLA2 neurotoxins block nerve terminals? *Trends Biochem. Sci.* **25**, 266–270 (2000).
52. M. Rigoni *et al*., Equivalent effects of snake PLA2 neurotoxins and lysophospholipid-fatty acid mixtures. *Science* **310**, 1678–1680 (2005).
53. M. Basselin *et al*., Imaging decreased brain docosahexaenoic acid metabolism and signaling in iPLA(2)β (VIA)-deficient mice. *J. Lipid Res.* **51**, 3166–3173 (2010).
54. Y. Cheon *et al*., Disturbed brain phospholipid and docosahexaenoic acid metabolism in calcium-independent phospholipase A(2)-VIA (iPLA(2)β)-knockout mice. *Biochim. Biophys. Acta* **1821**, 1278–1286 (2012).
55. Q. Zhou *et al*., Impairment of PARK14-dependent Ca(2+) signalling is a novel determinant of Parkinson's disease. *Nat. Commun.* **7**, 10332 (2016).
56. N. S. Hou *et al*., Activation of the endoplasmic reticulum unfolded protein response by lipid disequilibrium without disturbed proteostasis in vivo. *Proc. Natl. Acad. Sci. U.S.A.* **111**, E2271–E2280 (2014).
57. L. Gil-de-Gómez *et al*., Cytosolic group IVA and calcium-independent group VIA phospholipase A2s act on distinct phospholipid pools in zymosan-stimulated mouse peritoneal macrophages. *J. Immunol.* **192**, 752–762 (2014).
58. M. Carvalho *et al*., Effects of diet and development on the Drosophila lipidome. *Mol. Syst. Biol.* **8**, 600 (2012).

59. M. B. Hartig et al., Absence of an orphan mitochondrial protein, c19orf12, causes a distinct clinical subtype of neurodegeneration with brain iron accumulation. Am. J. Hum. Genet. **89**, 543–550 (2011).

60. V. Kainu, M. Hermansson, S. Hänninen, K. Hokynar, P. Somerharju, Import of phosphatidylserine to and export of phosphatidylethanolamine molecular species from mitochondria. Biochim. Biophys. Acta **1831**, 429–437 (2013).

61. C. Galvagnion et al., Lipid vesicles trigger α-synuclein aggregation by stimulating primary nucleation. Nat. Chem. Biol. **11**, 229–234 (2015).

62. L. Giehm, D. I. Svergun, D. E. Otzen, B. Vestergaard, Low-resolution structure of a vesicle disrupting α-synuclein oligomer that accumulates during fibrillation. Proc. Natl. Acad. Sci. U.S.A. **108**, 3246–3251 (2011).

63. M. Zhu, A. L. Fink, Lipid binding inhibits alpha-synuclein fibril formation. J. Biol. Chem. **278**, 16873–16877 (2003).

64. M. Pinot et al., Lipid cell biology. Polyunsaturated phospholipids facilitate membrane deformation and fission by endocytic proteins. Science **345**, 693–697 (2014).

65. B. Nuscher et al., Alpha-synuclein has a high affinity for packing defects in a bilayer membrane: A thermodynamics study. J. Biol. Chem. **279**, 21966–21975 (2004).

66. K. Pirc, N. P. Ulrih, α-Synuclein interactions with phospholipid model membranes: Key roles for electrostatic interactions and lipid-bilayer structure. Biochim. Biophys. Acta **1848**, 2002–2012 (2015).

67. M. Terada et al., The effect of truncation on prion-like properties of α-synuclein. J. Biol. Chem. **293**, 13910–13920 (2018).

68. G. Fusco et al., Direct observation of the three regions in α-synuclein that determine its membrane-bound behaviour. Nat. Commun. **5**, 3827 (2014).

69. S. I. Kubo, Membrane lipids as therapeutic targets for Parkinson's disease: A possible link between Lewy pathology and membrane lipids. Expert Opin. Ther. Targets **20**, 1301–1310 (2016).

70. R. P. Bazinet, S. Layé, Polyunsaturated fatty acids and their metabolites in brain function and disease. Nat. Rev. Neurosci. **15**, 771–785 (2014).

71. K. C. Hughes et al., Intake of antioxidant vitamins and risk of Parkinson's disease. Mov. Disord. **31**, 1909–1914 (2016).

72. L. M. de Lau et al., Dietary fatty acids and the risk of Parkinson disease: The Rotterdam study. Neurology **64**, 2040–2045 (2005).

73. M. S. Brenz Verca, A. Bahi, F. Boyer, G. C. Wagner, J. L. Dreyer, Distribution of alpha- and gamma-synucleins in the adult rat brain and their modification by high-dose cocaine treatment. Eur. J. Neurosci. **18**, 1923–1938 (2003).

74. J. Dong et al., Dietary fat intake and risk for Parkinson's disease. Mov. Disord. **29**, 1623–1630 (2014).

75. K. Trinh et al., Induction of the phase II detoxification pathway suppresses neuron loss in Drosophila models of Parkinson's disease. J. Neurosci. **28**, 465–472 (2008).

76. A. Tsubouchi et al., Mitochondrial protein Preli-like is required for development of dendritic arbors and prevents their regression in the Drosophila sensory nervous system. Development **136**, 3757–3766 (2009).

77. S. Bahadorani, P. Bahadorani, J. P. Phillips, A. J. Hilliker, The effects of vitamin supplementation on Drosophila life span under normoxia and under oxidative stress. J. Gerontol. A Biol. Sci. Med. Sci. **63**, 35–42 (2008).

78. M. J. Lee et al., The effects of hempseed meal intake and linoleic acid on Drosophila models of neurodegenerative diseases and hypercholesterolemia. Mol. Cells **31**, 337–342 (2011).

79. K. Yamamoto et al., Expression and function of group IIE phospholipase A2 in mouse skin. J. Biol. Chem. **291**, 15602–15613 (2016).

80. M. Masuda et al., Cysteine misincorporation in bacterially expressed human alpha-synuclein. FEBS Lett. **580**, 1775–1779 (2006).

MEDICAL SCIENCES